Unzipping DNA with Optical Tweezers: High Sequence Sensitivity and Force Flips

U. Bockelmann, Ph. Thomen, B. Essevaz-Roulet, V. Viasnoff, and F. Heslot
Laboratoire de Physique de la Matière Condensée, Ecole Normale Supérieure, 75005 Paris, France

ABSTRACT Force measurements are performed on single DNA molecules with an optical trapping interferometer that combines subpiconewton force resolution and millisecond time resolution. A molecular construction is prepared for mechanically unzipping several thousand-basepair DNA sequences in an in vitro configuration. The force signals corresponding to opening and closing the double helix at low velocity are studied experimentally and are compared to calculations assuming thermal equilibrium. We address the effect of the stiffness on the basepair sensitivity and consider fluctuations in the force signal. With respect to earlier work performed with soft microneedles, we obtain a very significant increase in basepair sensitivity: presently, sequence features appearing at a scale of 10 basepairs are observed. When measured with the optical trap the unzipping force exhibits characteristic flips between different values at specific positions that are determined by the base sequence. This behavior is attributed to bistabilities in the position of the opening fork; the force flips directly reflect transitions between different states involved in the time-averaging of the molecular system.

INTRODUCTION

During the last decade the field of single molecule studies on biological systems has strongly grown in importance. A very rapidly developing part of these activities concerns force measurements on DNA molecules (Allemand et al., 1998; Bockelmann et al., 1997, 1998; Bustamante et al., 2000; Clausen-Schaumann et al., 2000; Cluzel et al., 1996; Colton et al., 1994; Essevaz-Roulet et al., 1997; Léger et al., 1999; Rief et al., 1999; Smith et al., 1992, 1996; Wang et al., 1997) and force measurements on DNA-protein complexes (Davenport et al., 2000; Léger et al., 1998; Strick et al., 2000; Wuite et al., 2000; Yin et al., 1995).

A few years ago we reported on experiments where single DNA molecules are unzipped with a soft glass microneedle (Bockelmann et al., 1997, 1998; Essevaz-Roulet et al., 1997). Force signals have been recorded that reflect the proportion of G/C compared to A/T basepairs on an average scale of ~100 basepairs. A typical force versus displacement curve consists of a series of sawtooth-shaped features. This characteristic shape is explained theoretically in the frame of equilibrium statistical mechanics. The calculated physical effect, called molecular stick-slip motion, is a reversible molecular process caused by an interplay of the energy landscape given by the genomic sequence, the elasticities of molecule and measurement device, and the Brownian motion. Theoretical papers have been published that directly relate to our experimental configuration (Cocco et al., 2001; Lubensky and Nelson, 2000; Nelson, 1999; Thompson and Siggia, 1995; Viovy et al., 1994) and different groups have reported on AFM measurements of the force to separate the two strands of the DNA double helix (Colton et al., 1994; Rief et al., 1999).

Here, we report on DNA unzipping performed with a modified molecular construction and an optical trapping interferometer. The molecular construction is optimized for high stability by the incorporation of multiple attachment points and for high molecular stiffness by the use of relatively short double-stranded linker arms. An optical trapping interferometer is chosen because it combines high measurement stiffness (the trap compliance is almost negligible compared to the molecular compliance) with a sub-pN force resolution. In this configuration DNA unzipping can occur on a significantly more local scale than in our previous work. The effect of stiffness on the basepair sensitivity and the role of fluctuations are addressed. The paper focuses on displacement velocities below 1 μm/s. For this regime we expect the highest basepair sensitivity.

The experimental configuration is schematically presented in Fig. 1. The force measurements are performed in vitro on a molecular construction that is anchored between a glass microscope slide and a silica bead. The bead is held in an optical trap and the surface is laterally displaced, which leads to a progressive opening of the double helix. The force is obtained from a measurement of the bead position within the trap.

In the next section we explain the optical trapping interferometer and the calibration of the force measurements. Subsequent sections are devoted to the preparation steps of the molecular construction, the functionalization of the glass surfaces, and the theoretical description of DNA opening at thermal equilibrium. The Results section is divided into two parts. The first part is devoted to the basepair sensitivity of the unzipping signal. We show that the stiffness of the system is a key parameter for the sensitivity, as it strongly influences the amplitude of the molecular stick-slip motion. In the second part we consider fluctuations in the force signal and discuss a physical process we observed

Submitted July 6, 2001, and accepted for publication December 4, 2001.

Address reprint requests to Dr. Ulrich Bockelmann, Laboratoire de Physique de la Matiere Condensee, Ecole Normale Superieure, 24 rue Lhomond, 75005 Paris, France. Tel.: 33-1-4432-2565; Fax: 33-1-4432-3840; E-mail: ulrich@lpmc.ens.fr.

0006-3495/02/03/1537/17 $2.00

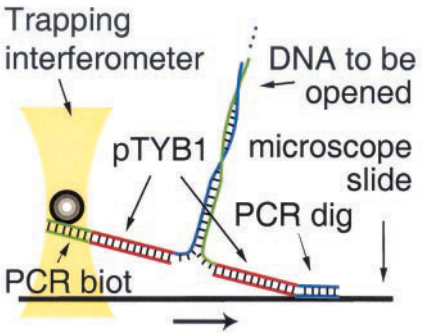

FIGURE 1 Schematic view of the single molecule configuration for unzipping DNA with optical tweezers.

for the first time when opening or closing DNA with the trapping interferometer: sudden flips between discrete force values, occurring at specific positions in the force signal. The reader uninterested in the setup and the preparations may skip the next two sections and directly go to the Theoretical Description and Results sections.

THE TRAPPING INTERFEROMETER

Experimental setup

We have built an optical trapping interferometer for the measurement of forces up to 100 pN but with subpiconewton resolution. In brief, a gradient beam optical trap is created by tightly focusing an infrared laser beam with a high-numerical-aperture microscope objective. The force acting on the bead is derived from an interferometric measurement of the position difference between the bead and the trap center. This position measurement is based on DIC (differential interference contrast) microscopy (Allen et al., 1969). About a decade ago, Denk and Webb (1990) measured the position of microscopic beads with this interferometric technique, and since then a number of groups have adapted different types of interferometric position measurements to optical tweezer experiments on single molecules (Allersma et al., 1998; Gittes and Schmidt, 1998a; Svoboda and Block, 1994).

Our setup is schematically shown in Fig. 2. It is based on a commercial inverted optical microscope (Zeiss Axiovert 100). The beam of a diode-pumped Nd:YAG cw laser (Coherent DPY321, 1W, 1064 nm) first passes a Faraday isolator to avoid back-reflection into the laser cavity that otherwise causes important intensity fluctuations. A telescope arrangement consisting of a pair of mirrors and a pair of convex lenses allows us to adjust independently the position and the angle of the beam. It also widens the parallel beam to a diameter slightly above the back plane aperture of the microscope objective (100×, N.A. = 1.25 oil immersion). The polarization of the linearly polarized laser light is rotated with a $\lambda/2$ plate to illuminate a first Wollaston prism with the electric field tilted by 45° with respect to the prism axis. This leads to an angular splitting

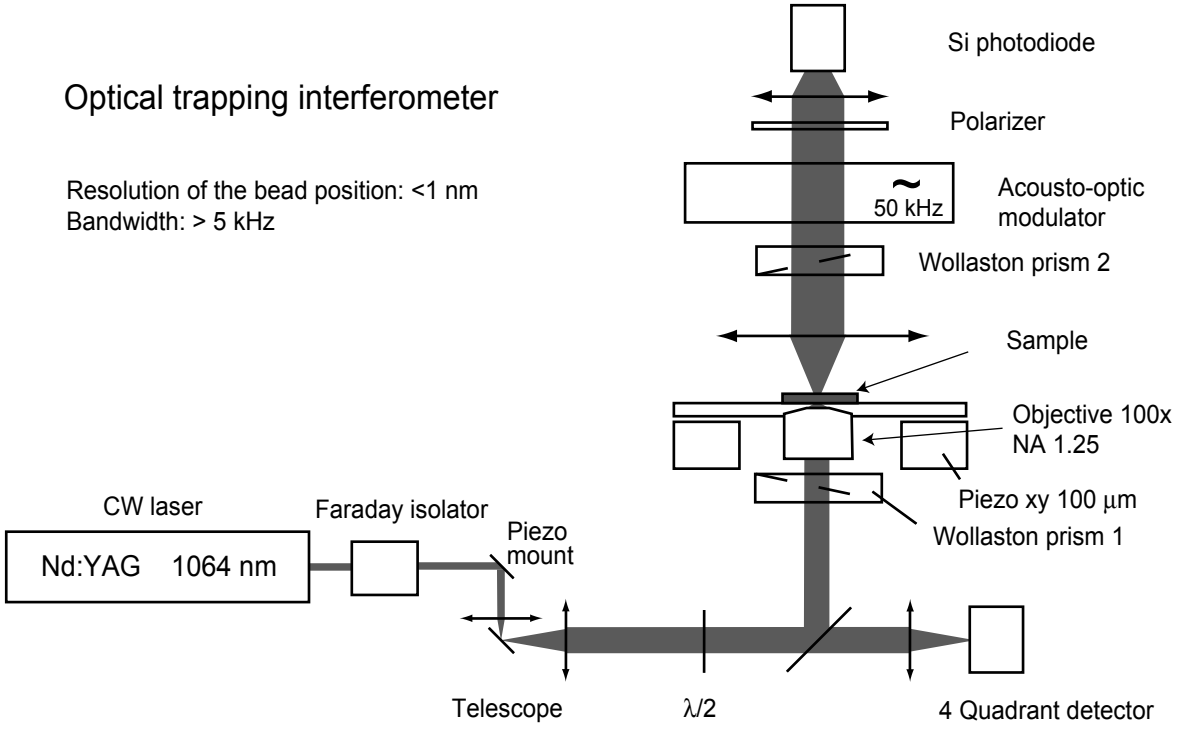

FIGURE 2 Schematic view of the optical trapping interferometer.

of the beam and, in the focal plane of the objective, to two partially overlapping, diffraction-limited spots of equal intensity. The two spots exhibit orthogonal linear polarization and a center-to-center distance of ~200 nm.

With this arrangement, silica beads (mean diameter of 1 μm) are trapped in aqueous solution, close to the center of the twin spot. As the 200-nm center-to-center distance is significantly smaller than the bead diameter, the effect of the optical trap along the axis of interest (the line connecting the two spots in the sample plane) is well-described by a simple harmonic potential of stiffness, k_{trap}.

To measure the lateral position of the bead in the trap, the transmitted light is collected by a condenser assembly and the two polarizations are recombined using a second Wollaston prism. With the bead in the center of the trap the recombined light is linearly polarized. However, a displacement along the line connecting the two focal points leads to a difference between the optical paths of the two beams and induces an ellipticity of the recombined light. This ellipticity is measured by a modulation technique, similar to an arrangement commonly used in ellipsometry (Azzam and Bashara, 1989). Our setup involves an acousto-optic modulator that introduces a ω = 50 kHz modulation of the refractive index along one direction and thus modulates the phase difference between the two polarization components. The modulated light passes a linear polarizer and is detected by a silicon photodiode. A voltage proportional to the light intensity is obtained with a custom-made current preamplifier. This voltage signal enters a lock-in amplifier with the 50 kHz signal of the modulator connected as reference. The amplifier output U_ω is proportional to the ellipticity of the light in front of the acousto-optic modulator. The analog signal passes a frequency adjustable anti-aliasing filter and is converted by a 16-bit ADC (IDSC816 card from Microstar Laboratory). The numerical data are written to a computer hard disk and analysis of the results is done off-line.

For the horizontal sample displacement, a piezo translation table with capacitive position sensors is mounted on top of a coarse *xy* translation stage. Piezo stage and position sensors are operated via a computer-adjustable feedback loop, which allows controlling the relative lateral sample position with nanometer precision and imposing different cycles of displacement. The vertical position of the microscope objective relative to the sample surface is measured with an inductive position sensor. Because the setup measures lateral bead displacements with subnanometer resolution and a bandwidth of several kilohertz, it is very important to reduce as far as possible mechanical perturbations and thermal drifts between trapping beam and sample. Most importantly, we use an optical table with active vibration isolation and protect the setup against air flow. In addition, to suppress small fluctuations of the lateral trap position arising from laser beam pointing, we have introduced a feedback loop in the excitation path that includes a piezo mirror mount and a quadrant photodiode. With these arrangements we are able to reduce the drift between the trapping beam and the sample position to ~10 nm/min. Although this is sufficient for many applications, the residual drifts still induce nonnegligible shifts between the experimental curves in our high-resolution unzipping measurements (see Results).

Calibration

We use three different approaches to calibrate the trapping interferometer. The first one, entitled "bead in a gel," allows us to relate the interferometer output to a piezo-controlled displacement of the bead in the trap and to determine the range where the interferometer output voltage and the displacement are proportional. The second configuration, "bead in an oscillating liquid," provides a direct measure of the constant of proportionality between the interferometer output and the force acting on the bead. The third configuration, entitled "Brownian motion of a captured bead," also gives this constant and, in addition, a measure of the trap stiffness. We describe the three techniques separately and then make some general remarks on the calibration of the trapping interferometer.

Bead in a gel

We use a polyacrylamide gel sufficiently dense to immobilize the beads. A bead is positioned in the center of the trap. This can be done by maximizing and symmetrizing the interferometer output voltage in response to a lateral bead oscillation of small amplitude. With the piezo table, the sample is oscillated laterally through the optical trap and the interferometer output U_ω is recorded as a function of the time-dependent position $x(t)$. For a bead positioned in the trap center, an oscillation perpendicular to the axis defined by the Wollaston prism leads to negligible output, while an oscillation along this axis leads to characteristic S-shaped curves. An example of such a curve is shown in Fig. 3. We observe that U_ω is proportional to x within an interval of ~300 nm around the trap center.

Bead in an oscillating liquid

In this method, a bead is held in the trap while the surrounding liquid buffer is moved by oscillating the sample holder. The viscous friction leads to an oscillating force on the bead. This calibration is facilitated by the small value of the Reynolds number:

$$R_e = \frac{\nu a \rho}{\eta} \cong 10^{-5} \quad (1)$$

where a is the bead diameter and ν, ρ, and η are, respectively, the velocity, mass density, and viscosity of the liquid.

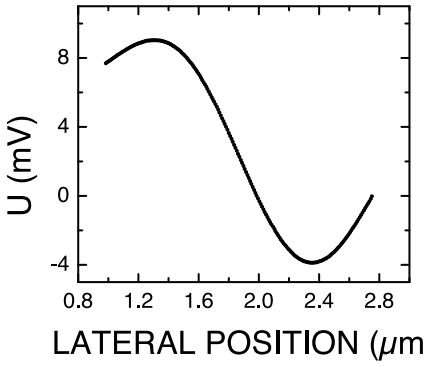

FIGURE 3 Bead in a gel. Interferometer output voltage U_ω recorded with a bead moving through the optical trap. At the trap center (corresponding here to a lateral position of ~1.85 μm) the output voltage is offset from zero on this graph. This offset can be tuned by a fine position adjustment of the first Wollaston prism.

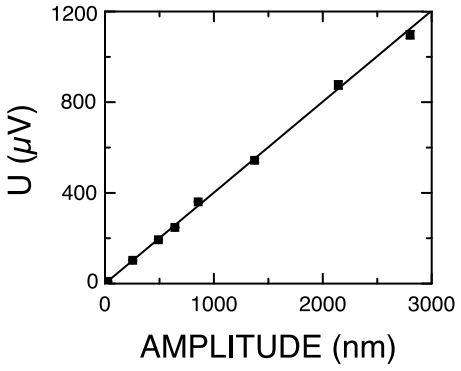

FIGURE 5 Bead in an oscillating liquid. Amplitude of the output voltage (voltage demodulated at ω and Ω) of the trapping interferometer as a function of the amplitude of the piezo stage. The liquid surrounding the bead of 1 μm in diameter is oscillated with a frequency of 20 Hz.

As a consequence, inertial forces are negligible. If, in addition, we neglect the stochastic Langevin force of the Brownian motion, the following differential equation is obtained:

$$k_{\text{trap}}x_{\text{b}} + \gamma\left(\frac{dx_{\text{b}}}{dt} - \frac{dx_{\text{l}}}{dt}\right) = 0 \qquad (2)$$

where the trap center defines the zero of the bead position x_{b}. We use k_{trap} for the trap stiffness, γ for the friction coefficient of the bead (given by Stokes' law without correction, as the bead is held at a height of several bead diameters above the glass slide), and x_{l} for the position of the liquid. To assure that the liquid moves rigidly with the piezo stage we fully enclose the liquid; i.e., the sample has no free meniscus.

Imposing a harmonic oscillation of the stage

$$x_{\text{l}} = x_0 e^{i\Omega t} \qquad (3)$$

of real amplitude x_0 and frequency Ω, we expect a bead oscillation of the form

$$x_{\text{b}} = A e^{i\Omega t} \qquad (4)$$

In general, the amplitude A has non-zero real and imaginary parts. From Eqs. 2–4 we obtain

$$A + i\Omega\tau(A - x_0) = 0 \qquad (5)$$

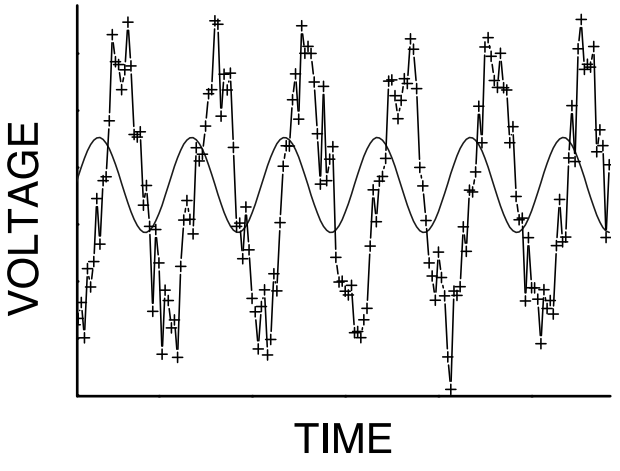

FIGURE 4 Bead in an oscillating liquid. The two curves show the measured interferometer output voltage U_ω (*noisy curve*) and the capacitive measurement of the sample position (*smooth curve*). We thus compare the displacements of the bead and the translation stage. The $\pi/2$ phase shift between U_ω and x_0, characteristic of the regime $\Omega\tau \ll 1$, is apparent. The noise in the bead position is due to the low frequency components of the Brownian motion. The interferometer voltage is measured with a lock-in amplifier at the reference frequency ω of the acousto-optic modulator. To extract the amplitude of the bead oscillation (Figs. 5 and 6) we use a second lock-in amplifier in series that demodulates at the frequency Ω of the oscillating translation stage.

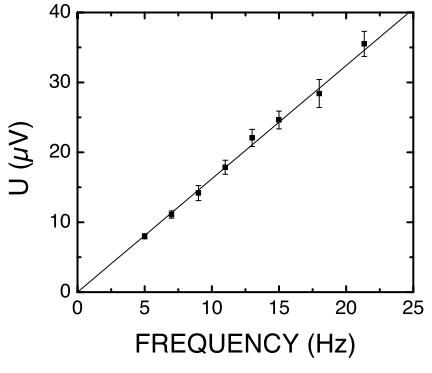

FIGURE 6 Bead in an oscillating liquid. Amplitude of the output voltage (voltage demodulated at ω and Ω) of the trapping interferometer as a function of the frequency of the imposed oscillation. The liquid surrounding the bead moves due to a stage oscillation of 75 nm in amplitude.

where we have defined

$$\tau = \frac{\gamma}{k_{\text{trap}}}$$

For the bead displacement follows:

$$x_{\text{b}}(t) = \frac{\Omega\tau x_0}{\sqrt{1+\Omega^2\tau^2}}\, e^{\text{i}(\Omega t+\pi/2-\varphi)} \tag{6}$$

with $\varphi = \arctan(\Omega\tau)$. Because x_{b} depends, via τ, on k_{trap}, this method could provide the stiffness as well as the calibration factor between the bead position x_{b} and the interferometer output U_ω. In practice, however, the product $\Omega\tau$ is small compared to one because τ is of the order of 10^{-4} s and kilohertz stage frequencies are difficult to reach. In the experimentally used regime of $\Omega\tau \ll 1$ the amplitude of the bead is given by

$$|A| = \tau\Omega x_0 \tag{7}$$

Multiplying Eq. 7 by k_{trap} and assuming that γ is known, we see that the amplitude $|F|$ of the force on the bead

$$|F| = k_{\text{trap}}|A| = \gamma\Omega x_0 \tag{8}$$

is proportional to the product of the frequency Ω and the amplitude x_0 of the stage. Therefore, only one independent parameter can be calibrated.

An example of the oscillating output voltage U_ω is shown in Fig. 4. At a given laser power we have performed two different series of measurements: 1) U_ω as a function of the amplitude x_0 at constant frequency Ω, and 2) U_ω as a function of Ω at constant x_0. The measured linear dependencies are presented in Figs. 5 and 6, respectively.

Brownian motion of a captured bead

In this case, the power spectrum of the Brownian motion of a trapped bead is measured with a spectrum analyzer. As this method has been presented in detail elsewhere (Gittes and Schmidt, 1998b; Svoboda and Block, 1994), we only give a brief description. The power spectral density S_{x} of the Brownian motion of a bead in a parabolic trapping potential of stiffness k_{trap} exhibits a Lorentzian shape

$$S_{\text{x}}(f) = \frac{k_{\text{B}}T}{\gamma\pi^2(f_{\text{c}}^2+f^2)} \tag{9}$$

with a cutoff frequency given by

$$f_{\text{c}} = \frac{k_{\text{trap}}}{2\pi\gamma} \tag{10}$$

As above, γ is the friction coefficient of the beads in water. For the power spectral density $S_{\text{x}}(f)$ of the bead position x we use the notation of reference (Svoboda and Block, 1994).

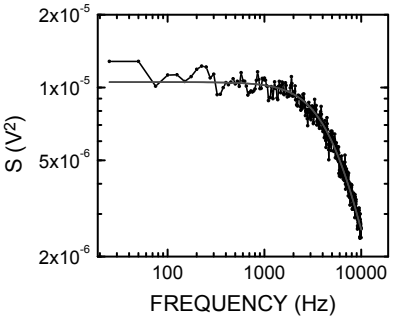

FIGURE 7 Brownian motion of a captured bead. Power spectral density of the interferometer signal U_ω for a glass bead of 1 μm in diameter. The bead is captured in water with a laser power of 700 mW (70% of our maximum laser power). The fit to a Lorentzian gives two parameters: the cutoff frequency f_{c} (here 5.7 kHz) and the area under the curve (here 4.72 mV^2/s).

Equation 9 describes the frequency distribution of the thermal fluctuations in the bead position. At low frequencies ($f \ll f_{\text{c}}$), the spectral density is constant, due to spatial confinement:

$$S_{\text{x}}(f \ll f_{\text{c}}) \cong \frac{4\gamma k_{\text{B}}T}{k_{\text{trap}}^2} \tag{11}$$

At high frequencies ($f \gg f_{\text{c}}$), $S_{\text{x}}(f)$ drops proportional to $1/f^2$. This dependence is characteristic of the diffusion in the absence of trapping.

In Fig. 7 a measurement of the frequency-dependent spectral density of a bead in water is shown. A fit to Eq. 9 allows us to determine two independent parameters, for instance the cutoff frequency f_{c} and the area under the curve. As shown in Figs. 8 and 9, both quantities show a linear dependence on the laser power. The trap stiffness is proportional to f_{c} (Eq. 10) and therefore also increases linearly with laser power. Afterward, the factor of proportionality between U_ω and the force on the bead is derived using f_{c} and the area under the spectral density curve.

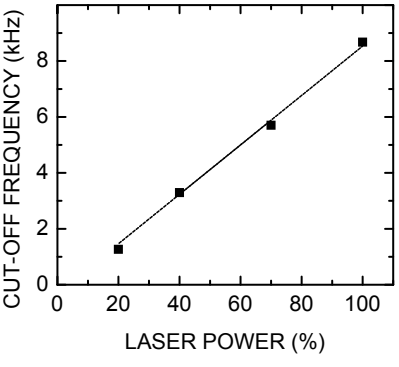

FIGURE 8 Cutoff frequency, obtained by a fit of the measured power spectral density to a Lorentzian, as a function of laser power (100% corresponds to 1 W at the laser).

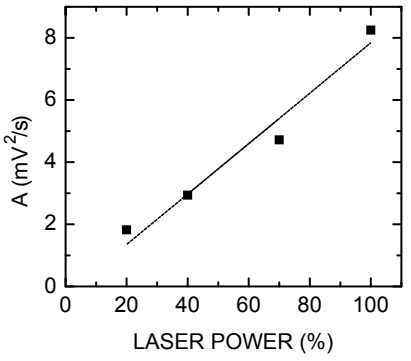

FIGURE 9 Area under the spectral density, obtained by a fit of the measured curve to a Lorentzian, as a function of laser power (100% corresponds to 1 W at the laser).

Conclusions on the three calibration techniques

It is a nontrivial task to determine precisely the systematic error of a calibration of a piconewton force measurement device. Therefore, it is valuable to compare the results obtained by different calibration methods. The first method is the most complicated of the three. The beads have to be immobilized by a sufficiently dense and optically homogeneous gel. The difference in the optical properties of the gel and the aqueous buffer is difficult to evaluate and may be nonnegligible. The correct positioning of the bead is critical. Although we consider this technique less for direct calibration, we find it valuable because it allows us to measure the linearity range of the trapping interferometer. We also use a variant of this approach where a bead immobilized on the glass slide is tracked under liquid. The second method, bead in an oscillating liquid, directly relates U_ω to the force on the bead, is relatively easy to implement, and allows a calibration for all laser powers. The calibration derived from the amplitude series (Fig. 5) agrees to within 7% with the one derived from the frequency series (Fig. 6). Only the third method allows us to measure the trap stiffness. For the precision of the force calibration this last method is comparable to the second one, except at high laser power, where the cutoff frequency approaches the bandwidth of the interferometer.

The two calibration parameters, the trap stiffness k_{trap}, and the ratio between interferometer output and bead displacement increase linearly with the laser power P (for the linear power dependence of the trap stiffness, see also Simmons et al. (1996)). With $P = 700$ mW we obtain a stiffness $k_{trap} = 250$ pN/μm for silica beads of 1 μm diameter in H_2O. The force calibration obtained by methods two and three differ by ~10%. We also find a nonnegligible bead-to-bead variation of the calibration factor. Performing oscillation amplitude series on 64 different beads, we obtained calibration factors in a $\pm$10% interval around the average value.

SAMPLE PREPARATION

The molecular construction

Overview

To mechanically open a DNA molecule, the device that will separate the strands and measure the force has to be adapted to the DNA interstrand spacing of ~2 nm. The silica beads, used as a handle in the present case, are of micrometer size. Much smaller beads would not allow applying sufficient trapping force at reasonable laser power. A specific DNA construction has been designed where both strands of the DNA to be opened are prolongated by linker arms of ~2.5 μm length each (Fig. 10). These linker arms consist of double-stranded (ds) DNA which contain, close to one of their extremities, multiple, modified basepairs. One type of linker is modified with biotin groups to react to streptavidin-coated beads, the other type is modified with digoxigenin groups to react to anti-digoxigenin-coated microscope slides. The body of the linker arms derives from a pTYB1 cloning vector and the modified part is obtained by PCR. The DNA to be opened is from the bacteriophage λ. Synthetic oligonucleotides are used to connect the different elements.

The molecular construction of the present work contains two linker arms, in contrast to our earlier studies where a

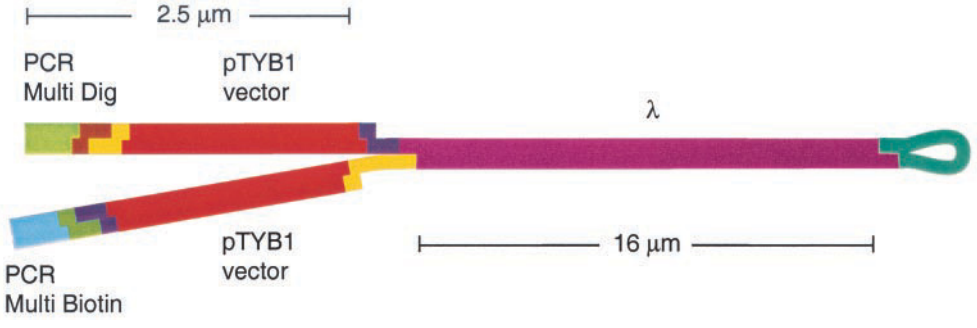

FIGURE 10 Schematic view of the molecular construction.

single linker was used. The aim is to reduce as far as possible nonspecific interactions between the molecule to be opened and the silica bead or the microscope slide. The total length of the two linker arms in series is three times smaller than the single 15-μm λ-DNA linker used in the earlier work, leading to an increased stiffness of the molecular construction. We also introduced multiple attachment points at each extremity of the construction rather than single attachments to increase the stability of the molecule-surface linkages. The preparation steps, described in detail in the following three subsections, use a number of techniques currently used in molecular biology, such as DNA digestion, hybridization and ligation, PCR, purification on spin columns, etc.

Preparation of modified DNA by PCR

An 1890-bp DNA fragment is PCR-amplified from the 6369-bp fragment of a commercial λ/*BstE*II digest. The sequences of the two flanking oligonucleotides are 5′-AGG GGT ACA CGA GAA CCA (18-mer, XHO3) and 5′-GAT GAT GCG GGA CCA GCC (18-mer, XHO5). The amplified fragment contains a unique *Xho*I restriction site in the middle. The following PCR protocol is run on a commercial thermocycler: initiation of 3 min at 94°C, 30 denaturation/hybridization/extension cycles with 30 s at 94°C, 30 s at 57°C, and 2 min at 72°C. The last step of the PCR reaction is done for 3 min at 72°C. For 50 μl volume we use 10 ng λ/*BstE*II digest, oligos at 20 pmol each, dNTPs at 50 μM each, dUTP-biot (or dUTP-dig) 5 μM, 0.5 μl TAQ polymerase. The PCR product (typically 1–2 μg for a 50 μl PCR volume) is purified on a Qiaquick spin column (QIAGEN), *Xho*I-digested (overnight), and purified again on the same column. Despite long incubation complete digestion is not achieved, probably because the enzyme does not cut the DNA molecules that have modified bases in the recognition sequence.

Assembly of the DNA linker arms

The 7280-bp ds-DNA is prepared by overexpressing a pTYB1 cloning vector (New England Biolabs) in *Escherichia coli*. Purification of this circular DNA is done on a macroporous silica ion exchange column (nucleobond AX, Macherey-Nagel, Germany). The sample is *Sal*I-digested, phenol/chloroform-purified, and ethanol-precipitated. Afterward, it is digested by *Kpn*I and purified on a centricon-100 (Amicon) spin column. This purification is chosen to remove the 48-bp stretch cut from the circular DNA to avoid recyclization of the linearized DNA during subsequent ligation steps.

Two different types of ds-DNA linkers are prepared by annealing pairs of partially complementary oligonucleotides. The first, named LINKDIG, involves the oligonucleotide sequences 5′-AGA GAA CAG TGA CAT AAA CTA GGA GAT TG (29-mer, ANTIBANAKPN) and 5′-ATG TCA CTG TTC TCT GTA C (19-mer, KPNVEC). The second, named LINKBIOT, involves the sequences 5′-TGA CAT TAG AGA CAG (15-mer, KPNVECS) and 5′-AGG TCG CCG CCC CAA TCT CCT AGT AAA AAG TGT CTC TAA TGT CAG TAC (48-mer, BANAKPN). The final assembly of a linker arm consists of ligating a *Xho*I-digested PCR fragment to the *Sal*I extremity of a linearized pTYB1 vector DNA and an oligo-based ds-linker to the *Kpn*I extremity. One reaction involves the PCR product obtained with digoxigenin-modified nucleotides, the linker LINKDIG, and the linearized pTYBI DNA. The other reaction involves the biotin-modified PCR product, the linker LINKBIOT, and the linearized pTYBI DNA. Both ligations are done in a total volume of 75 μl digestion buffer 3 (NEB) completed with ATP to 1 mM final concentration and PEG to 15% (final w/v). The reaction is done with 1 pmol PCR fragments, 1 pmol pTYB1, 20 pmol oligo ds-linker, 0.5 μl *Sal*I restriction endonuclease (10 units), 0.5 μl *Xho*I restriction endonuclease (10 units), and 1 μl T4 DNA ligase (400 units). Ligation is done overnight at 16°C. The *Xho*I enzyme is included to avoid formation of dimers of PCR fragments. The *Sal*I enzyme is included to avoid formation of dimers of pTYB1 molecules on the *Sal*I cohesive end. The ligation products are purified on centricon-100 spin columns.

Preparation of the λ DNA and final ligation

For the molecule to be opened, we have chosen the commercially available λ-DNA (48,502 bp). We covalently cap one cohesive end by ligation with a hairpin oligonucleotide 5′-GGG CGG CGA CCT AGC GAA AGC T (22-mer, ACOS-HAIRPIN). For a final volume of 75 μl, 500 fmol λ-DNA and 30 pmol ACOS-HAIRPIN oligonucleotides are incubated in ligase buffer (without ATP) for 4 min at 65°C and afterward slowly cooled. This temperature treatment is intended to linearize the λ-DNA and to hybridize the hairpin oligo to one of the two 12-bp cohesive ends. ATP and ligase are added and ligation is done overnight at 16°C. The ligation product is purified on a centricon-100 (Amicon) spin column.

The final assembly is done in a volume of 370 μl with 15% PEG. We first pool the ligated biotin linker arms and the λ-DNA ligation (200 fmol each). This sample is incubated in ligase buffer (without ATP) 30 min at 55°C for annealing. Afterward, 200 fmol of the ligated digoxigenin linker arms are added and a second annealing step is performed, 1 h at 40°C. The sample is gradually cooled to 16°C for 6 h. ATP and ligase are added and ligation is performed overnight at 16°C. The ligase is heat-inactivated and the sample is purified on a centricon-100 spin column. The molecular construction is stored in a freezer in TE buffer and can be used for several months.

Surface treatment

To attach the digoxigenin-functionalized part of the molecular construction, we have coated glass slides with anti-digoxigenin, as described below. The biotin groups are attached to commercial streptavidin-coated beads (1 μm diameter, Bangs), as described in the following section.

Standard microscope glass slides are put into an ozone atmosphere for 1 h, to oxidize organic surface contaminations. After this cleaning step, the slides are silanized. First, 10 μl of a vinyl-functionalized silane (triethoxysilyl-modified polybutadiene) are dissolved in 1 ml methyl ethyl ketone. Then 2 μl Tween (10% in H_2O) and 10 μl H_2O are added and the solution is deposited on the slides and allowed to react at room temperature for 20 min without drying. The slides are then rinsed with toluene and baked 2 h at 150°C. These slides are stored dry at room temperature and can be used for several months.

At this stage, a small plastic ring is glued on each slide. In the following surface reactions, liquid volumes of the order of 10 μl are deposited inside the ring, and this sample is covered with a circular glass slide to avoid evaporation. We then proceed to a statistical polymerization based on a mixture of acrylic and maleic acids. Covalent binding is obtained by a reaction between the carbon double bonds of the silane and polymer molecules. The linear polymers introduce amide and carboxyl groups and lead to a negatively charged, hydrophilic surface. The preparation is based on standard protocols of acrylamide gels for electrophoresis (Sambrook et al., 1989). A typical polymerization reaction contains 3% (w/v) acrylic acid, 0.05% (w/v) maleic acid and, as catalyst and initiator, 0.1% (w/v) persulfate and 0.1% (v/v) TEMED (*N*,*N*,*N*′,*N*′-tetramethylethylenediamine) in deoxygenated water. Polymerization between the silanized slide and a covering slide is allowed for 1 h at room temperature. The covered slides are stored in a refrigerator in a humid environment and can be used for several months.

For the subsequent coupling of the anti-digoxigenin antibody, the covering slide is removed and the surface rinsed with H_2O. The carboxyl groups of the polymer layer are activated with an aqueous solution containing 200 mM EDC (1-ethyl-3-(3-dimethylaminopropyl)carbodiimide) and 50 mM NHSS (*N*-hydroxysulfosuccinimide) for 5 min. The surface is rinsed again and a solution (0.5 mg/ml in PBS) of an antibody directed against digoxigenin is incubated for 5 min. The surface is deactivated by incubating 7 min with an ethanolamine solution (1 M, pH 8.5). The anti-digoxigenin-coated surface is then rinsed with H_2O and stored under a blocker solution (casein in PBS, Pierce).

Final steps before force measurement

A small volume of the dilution containing typically 10^{-17} mol of the molecular construction is deposited on an anti-digoxigenin-coated slide, the surface is covered, and the sample incubated for 10 min at room temperature. This gives enough correctly attached molecular constructions for multiple force measurements on a given surface, and the DNA concentration is still sufficiently low to avoid non-specific DNA-surface interactions and attachment of beads via more than a single DNA molecule. About 150 μl PBS (pH 7, 10 mM phosphate, 150 mM NaCl), containing the streptavidin-coated silica beads, are added. The sample is mounted on the translation stage of the trapping interferometer. After ~10 min, we induce a rotation of the circular slide covering the sample by applying an air current at an oblique angle on one edge of the circular slide. This entails a rotation of the slide and of the liquid, and we exploit the following two effects. First, the flow induces a viscous force that allows us to identify the correctly attached beads. The latter display superposed on Brownian motion, a characteristic displacement that corresponds to the total length of the linker arms in the molecular construction (~5 μm in the present case). The second effect of the liquid rotation is that the nonattached beads on the bottom of the sample progressively concentrate close to the rotation axis. This way, we can significantly reduce the number of free beads in the vicinity of the measurement position and we avoid capturing more than a single bead in the force measurement. Once a correctly attached bead is identified, the rotation is stopped, the trap is laterally positioned, and the bead is captured by switching on the laser. Immediately afterward, force curves can be measured by laterally displacing the sample with the piezo stage and recording the interferometer output. The axial sample position is kept constant; typically the bead is held in the liquid at a height of 2–4 μm above the glass slide.

THEORETICAL DESCRIPTION

We have developed a theoretical description of DNA unzipping with a force measurement device. It is based on equilibrium statistical mechanics and involves the following four energy contributions.

The first energy, called $E_{\mathrm{DNA}}(j)$, describes the work necessary to separate the two strands of the DNA double helix from the basepair of index 1 to the base pair of index j. This energy is derived from the work of SantaLucia (1998), who compiled data from melting experiments on oligonucleotides and DNA polymers, and who provides the binding energies of the different DNA basepairs, including nearest-neighbor contributions.

The second energy, called E_{ext}, is associated with the elasticity of the single-stranded and double-stranded parts of the molecular construction. The elasticity of the single-stranded parts (which increase in length as the opening progresses) is described in a freely jointed chain model with entropic and enthalpic contributions (Smith et al., 1996). The elasticity of double-stranded DNA is treated in a worm-

like chain model (Smith et al., 1992; Odijk, 1995) with parameters taken from Wang et al. (1997). Our description of the elasticity of the single- and double-stranded parts of the molecular construction is compatible with data from the literature (Allemand et al., 1998; Smith et al., 1996; Wang et al., 1997) and with measurements that we have performed pulling single DNA molecules from opposite ends.

The third energy, called E_{trap}, is the potential energy of the bead in the trap; $E_{\text{trap}} = k_{\text{trap}}x^2/2$. The force-induced displacement of the bead is given by $x = x_0 - \delta_1 - \delta_2$, the difference between the sample displacement x_0, the length δ_1 of the DNA strand attached to the microscope slide, and the length δ_2 of the DNA strand attached to the bead.

The fourth energy is the thermal energy kT. It leads to the Brownian motion and directly enters the statistical weight in our calculation of the thermal averages in the canonical ensemble (Eq. 12). In this article we use $T = 300$ K and do not consider temperature variations. The thermal average of an observable A is calculated according to

$$\langle A \rangle = \frac{\sum_{j,\delta_1,\delta_2} A(j, \delta_1, \delta_2) e^{-E_{\text{tot}}(j,\delta_1,\delta_2)/kT}}{\sum_{j,\delta_1,\delta_2} e^{-E_{\text{tot}}(j,\delta_1,\delta_2)/kT}} \quad (12)$$

with the total energy given by

$$E_{\text{tot}} = E_{\text{DNA}}(j) + E_{\text{ext}}(j, \delta_1, \delta_2) + E_{\text{trap}}(\delta_1 + \delta_2) \quad (13)$$

The theoretical description has been published in closer detail elsewhere (Bockelmann et al., 1998). In our earlier work we compared calculations to unzipping measurements performed with soft glass microneedles, and we neglected the elasticity of double-stranded DNA and nearest-neighbor contributions to the binding energy of the basepairs.

No velocity dependence is included in our theoretical description. For the displacement velocities of the measurements considered in this article, Stokes' formula gives a frictional force on the bead well below 1 pN. When we unzip DNA with the optical tweezer setup at velocities above 1 μm/s, the opening force increases with velocity. This velocity dependence increases with the length of the DNA to be opened, suggesting that it arises from viscous friction of the rotating DNA tail (Ph. Thomen et al, manuscript in preparation). Without considering rotational friction, Cocco et al. (2001) have theoretically studied force and kinetic barriers to unzipping DNA and predict an increase in the opening force starting at loading rates above $10^{5.5}$ pN/s. However, with the stiffness range of optical tweezers (typically 50–300 pN/μm) and displacement velocities below 1 μm/s, we are more than three orders of magnitude below such loading rates.

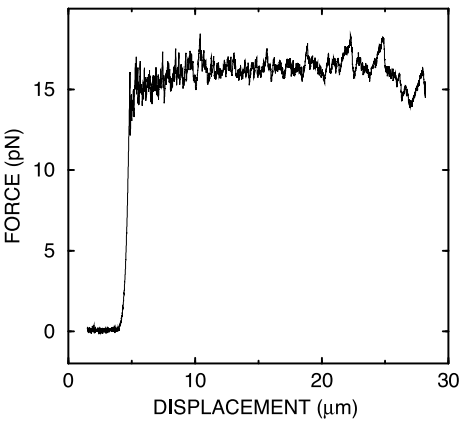

FIGURE 11 Force versus displacement curves corresponding to mechanical unzipping of a single λ-phage DNA molecule. The trace is recorded during opening of the double helix with a constant displacement velocity of 1 μm/s (sampling rate of 400 Hz, aliasing filter cutoff frequency of 176 Hz).

RESULTS

Relation between stiffness and basepair sensitivity

In Fig. 11 we present a force versus displacement curve measured upon opening the molecular construction. The force F starts to rise sizably when the displacement approaches the total crystallographic length of the double-stranded linker arms. Around 10–15 pN the force ceases to increase and the regime of increasing elastic DNA deformation changes into a regime of mechanical unzipping, where the two strands of the DNA molecule separate and the opening fork progresses through the genomic sequence with ~1000 bp per μm of additional displacement. In the unzipping regime, which for the λ-DNA extends over a displacement range of almost 50 μm, the force exhibits a very rapid variation with a typical amplitude of ~10%. This force variation is due to the differences in the pairing and stacking energies among the different basepairs, and thus reflects the known sequence of the λ-DNA in the molecular construction. As expected from the relative stability of the Watson-Crick basepairs, a G/C-rich region corresponds to higher unzipping force than an A/T-rich one (Bockelmann et al., 1997, 1998; Essevaz-Roulet et al., 1997). This result was confirmed by Rief et al. (1999), who derived an unzipping force of 10 pN from AFM measurements on a poly-A/T oligonucleotide duplex and a value of 20 pN from measurements on a poly-G/C duplex.

Fig. 12 provides a zoom into the force signal of a 100 nm/s measurement for three different displacement intervals. The experimental data (*bottom curves*) are compared to a calculation (*upper curves*, upshifted by 4 pN for presentation and based on the assumption of thermal equilibrium as described in the preceding section). The force signal is composed of a succession of sawtooth-like structures. For

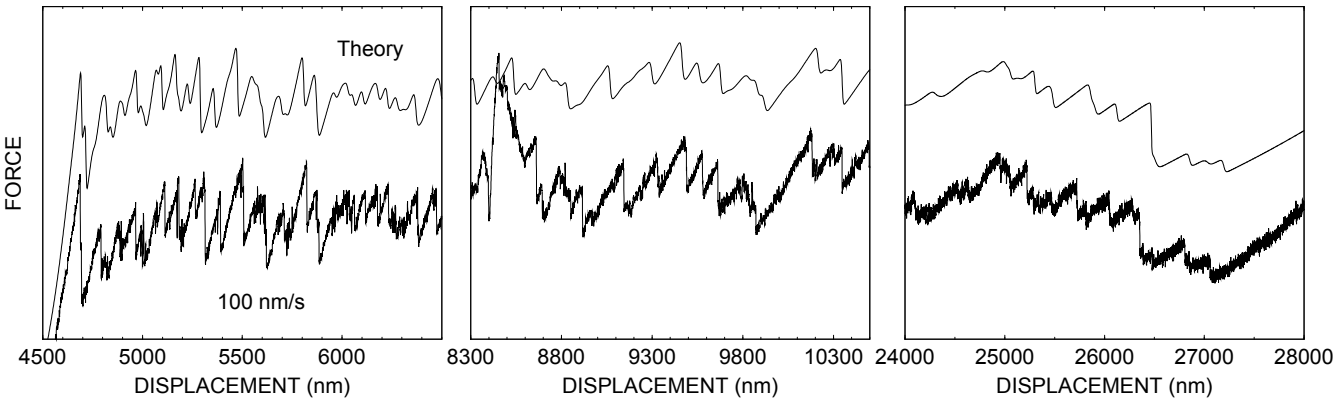

FIGURE 12 Evolution of the unzipping force signal with increasing displacement. The measured curve (*bottom*) corresponds to an opening performed with a displacement velocity of 100 nm/s (sampling rate, 400 Hz; anti-aliasing filter cutoff frequency, 176 Hz). The upper curve is the result of a calculation assuming thermal equilibrium, as described in the text. Three different displacement intervals are shown. They roughly correspond to opening from basepair 1 to 1800 (*left*), 3600 to 5800 (*middle*), and 19,600 to 24,100 (*right*). The measured and the calculated curve exhibit the same scaling but are vertically displaced for convenience. The feature around 8500 nm is a nonreproducible experimental event. Such events occur exceptionally and we do not know the origin.

a given additional displacement the opening progresses a little during the gradual rise in force, and a lot during the drop in force. This behavior can be understood in the frame of equilibrium statistical mechanics as an interplay of the complex energy landscape caused by the DNA base sequence, the Brownian motion, and the compliances of the molecule and the optical tweezer (Bockelmann et al., 1997, 1998).

One way to quantify the sensitivity of the force signal to the base sequence is to consider the calculated variance in the number j of opened basepairs (amplitude of the thermal breathing of the opening fork). This variance var j exhibits a rapid variation as a function of the local sequence (see Bockelmann et al., 1998; Fig. 5). During opening of the first 2000 basepairs (left graph of Fig. 12), the stick phases correspond to an amplitude of 5–10 bp, while during the slip events the averaging involves 20–50 bp. Assuming a constant sequence, we analytically find that var j is proportional to $k_{\mathrm{tot}}^{-1/2}$. The total local stiffness of the system is given by

$$k_{\mathrm{tot}}^{-1} = k_{\mathrm{ss}}^{-1} + k_{\mathrm{ds}}^{-1} + k_{\mathrm{trap}}^{-1} \tag{14}$$

with k_{ss}, k_{ds}, and k_{trap} being the local stiffness at the opening force of the single-stranded DNA, the double-stranded DNA, and the measurement device, respectively. In the present case, k_{tot} is limited by the molecule and not by the measurement device. The stiffness k_{tot} decreases with increasing displacement because the length of the ss-DNA increases. This leads to the systematic decrease in the slope of the rising part of the sawteeth in Fig. 12 (notice the different horizontal scale of the rightmost graph). Concomitant with that, the average size of the sawteeth increases, the density of features decreases, and the average noise amplitude increases.

In Fig. 13 we directly compare the unzipping signal of our earlier microneedle experiment with the one of the trapping interferometer. Opening the same sequence of basepairs, the optical trap data give a significantly higher density of structures in the force versus displacement curve. The trapping interferometer is about two orders of magnitude stiffer than the glass microneedle used in the earlier work (250 versus 1.7 pN/μm) and the two ds-linker arms of the new molecular construction are about three times stiffer than the original λ-DNA linker (total length of 14,560 bp versus 48,502 bp). As shown in Fig. 13, our calculations indeed predict that the resulting increase in total stiffness leads to the experimentally observed gain in basepair sensitivity. In the microneedle case, the amplitude of the molecular stick-slip motion is stronger. This is exemplified by the presence of pronounced steps and plateaus in the curve describing the progression of the opening fork with increasing displacement (upper part of Fig. 13).

A different way to investigate basepair sensitivity is to study the effect of mutations in the DNA sequence on the calculated force signal. In Fig. 14 we present force curves calculated for opening a λ-DNA sequence with different single-basepair mutations. We have chosen the positions of the mutations to be located on small features of the force signal, because in the presence of experimental drift, the modification of a small feature would probably be easier to detect than a change of same amplitude in a smoother part of the force curve. In the calculations a different base sequence always gives a different force curve, and any single-basepair mutation is detectable. Even the interchange of the bases of a given pair (see example 189 C → G) induces a modification because the binding energy depends not only on the local basepair, but also on the neighboring bases (SantaLucia, 1998). The twin peak at 5100 nm dis-

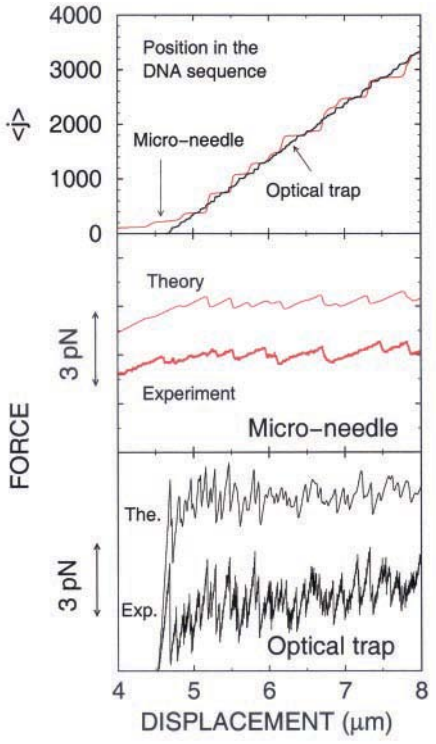

FIGURE 13 Comparison of an unzipping signal measured with a soft microneedle (*middle*) and a signal measured with the trapping interferometer (*bottom*). Each experimental curve is compared to a calculation based on the assumption of thermal equilibrium. The microneedle data have been recorded with a displacement velocity of 20 nm/s, the optical trap data with a velocity of 200 nm/s. Both measurements correspond to opening the first 3200 basepairs of the λ-DNA. For both cases the average number of opened basepairs $\langle j \rangle$ has been calculated as a function of displacement and is presented in the upper part of the figure (position in the DNA sequence).

placement can be suppressed in the calculation by changing basepair 393 from A/T to C/G. Similarly, the small peak occurring at 4800 nm displacement disappears upon a mutation C/G to A/T on basepair 189. The small peak at 5700 nm is either reinforced or replaced by a deep valley by single-basepair mutations at position 1079 (T/A to G/C) and 1080 (C/G to A/T). As illustrated for basepair 189, a mutation from a C/G to an A/T pair (or vice versa) typically induces a stronger change in the force signal than a basepair reversal (C/G to G/C). These theoretical considerations already indicate that the different mutations that induce biological phenotypes (replacements, deletions, insertions, mispairings) will be more or less difficult to observe in the unzipping configuration. The difficulty will decrease with increasing number of modified basepairs and will also depend on the type(s) of the mutation(s) and its (their) local sequence environment.

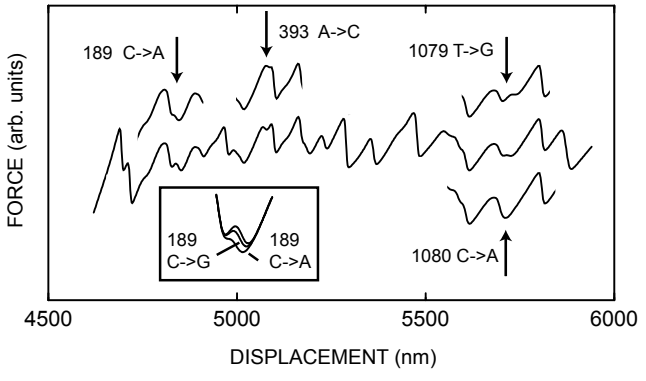

FIGURE 14 Calculated effect of different single basepair mutations on the force versus displacement curve. The superposition of three curves presented in the inset gives an enlarged view on the effect of a (C/G to A/T) mutation and of a (C/G to G/C) inversion with respect to the nonmutated sequence.

Experimentally, the basepair sensitivity also depends on the quality of the force measurement, in particular on the signal-to-noise ratio and the proper control of the relevant experimental parameters. The detection of very local sequence events becomes increasingly difficult with increasing amplitude of the thermal motion of the opening fork, and hence with the length of the DNA to be opened. However, the precision of the force measurement can be improved by decreasing the displacement velocity that allows low-pass-filtering the Brownian motion with increasing efficiency. Therefore, the noise on the experimental force curves can be (and in our measurements sometimes is) smaller than the calculated thermal variance of the force. Brownian motion therefore does not represent a fundamental limitation, but may nevertheless induce a very serious experimental difficulty. For instance, residual drifts, which are often due to changes in thermal expansion of the setup, have to be controlled on increasingly long time scales if increasing time-averaging of the signal is needed to low-pass-filter the Brownian motion. In this sense, the experimental performances determine to which precision the thermal average of the force is measured and what sensitivity can be achieved in terms of the genomic sequence.

Our measurement configuration allows us to perform several measurements on the same molecule. The double helix reforms spontaneously when the direction of the stage motion is reversed and, after this closing, a new opening measurement can be engaged. We observe no systematic difference in the degree of reproducibility between two consecutive opening measurements on the same molecule with respect to the degree of reproducibility between two recordings performed on two different molecules. This shows that under the present conditions the DNA double helix is able to renaturate to its native B-form under an external force in the 10–15 pN regime. In Fig. 15 we compare three measurements (E1–E3) and a calculation (Th), corresponding to the opening of the first 2500 bp of the λ-DNA. A comparison of Figs. 14 and 15 suggests that our measurements provide rather local information on the base sequence. The twin peak at 5100-nm displacement is

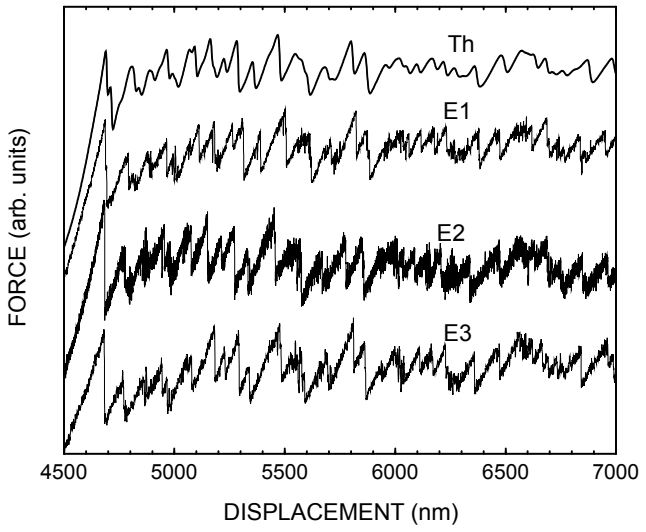

FIGURE 15 Variation of the opening force during the first 2500 nm of the opening. Measurements on two different molecules are presented. One has been opened with a velocity of 100 nm/s (E1), the other one with 50 nm/s (E2), and 200 nm/s (E3). For all three measurements we used a sampling rate of 400 Hz and a cutoff frequency of 176 Hz. The calculated curve (Th) is based on the assumption of thermal equilibrium and therefore corresponds to the theoretical limit of zero displacement velocity.

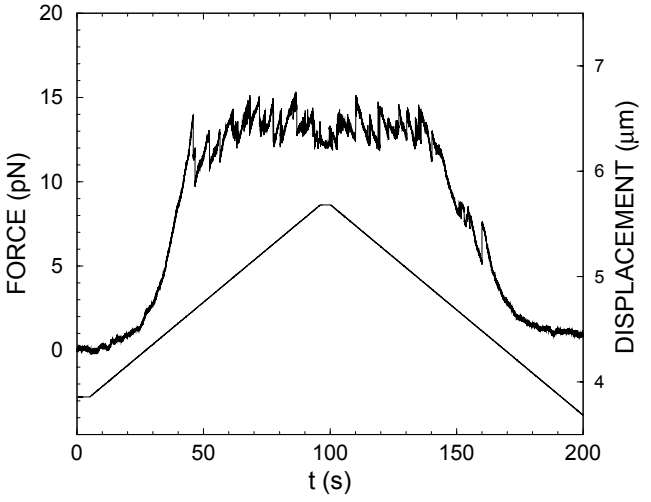

FIGURE 16 Opening and closing a DNA molecule with a displacement velocity of 20 nm/s. The force signal of the trapping interferometer (*upper curve*) and the displacement of the translation stage (*lower curve*, measured with a capacitive position sensor) are shown as a function of time. The data are recorded with a sampling rate of 100 Hz and an anti-aliasing filter cutoff frequency of 44 Hz.

weakly resolved in measurements E1 and E3. This structure can be suppressed in the calculation by changing basepair 393 from A/T to C/G. The small peak in a valley occurring at 4800 nm displacement is present in measurements E1 and E2, and disappears upon a mutation C/G to A/T on basepair 189. The small peak at 5700 nm may be guessed in the noise of the experimental traces E1 and E2. In the calculation this feature is either reinforced or replaced by a deep valley by single-basepair mutations at position 1079 (T/A to G/C) and 1080 (C/G to A/T).

The differences between the measurements presented in Fig. 15 are only partly due to the different displacement velocity. Our measurements show a certain degree of nonreproducibility. On the one hand, this can have several experimental reasons, in particular thermal drifts of the setup, mechanical, acoustic, and electrical noise, spatial inhomogeneity of the sample transmission, etc. A major remaining limitation of our setup arises from residual drifts between the trapping beam (position controlled with respect to the commercial microscope stand) and the part of the (custom-built) coarse displacement stage that holds the piezo stage. This probably induces the small shifts between the experimental curves. On the other hand, there is the possibility of an intrinsic statistical variation between different force measurements, even in the regime of small displacement velocity. In the following section, a possible mechanism for a statistical variation of the force signals is discussed.

Force fluctuations: bistability of the opening fork

In this section we consider the fluctuations in the force signal occurring at low displacement velocity. In the measurement presented in Fig. 16 a DNA molecule is opened with a stage velocity of 20 nm/s, the displacement is stopped for a short time, and we let the molecule close itself by moving back the stage (again with a velocity of 20 nm/s). A rough mirror symmetry appears between the left and right halves of the figure. In particular, we note that the orientation of the sawtooth structures is reversed in time during the closing of the molecule, and that there is no significant reduction of the force during closing as compared to the opening. Of course, our theoretical description predicts a perfect symmetry between opening and closing because it assumes that thermal equilibrium is reached at each instant t. The presented experimental data show a significant deviation from this prediction. In Fig. 17 we have directly superposed the opening and the closing data. There are regions where the two curves are similar, and there are regions where they differ. In general, a more important difference is observed between an opening and a closing measurement than between two opening measurements. We also find that the degree of reproducibility between two closing measurements is typically smaller than the one between two opening measurements. This indicates that equilibrium is not systematically reached, in particular during closing (even at the small velocity of 20 nm/s, corresponding to zipping 20 basepairs per second on average). In Fig. 16 the molecule starts to open at a force between 10 and 15 pN, while during closing important sawtooth structures persist down to 5 pN. Clearly, such differences are not

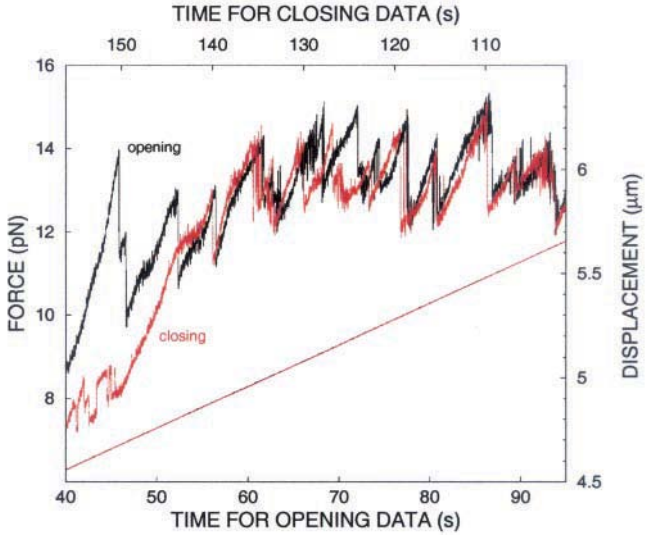

FIGURE 17 Comparison of the force signals recorded during the opening and during the closing phase of the measurement of Fig. 16. The lower horizontal time scale corresponds to the opening (*upper dark curve* for the force, *lower dark curve* for the displacement). The closing signals (*red curves*) are presented with a reversed time axis (time increase from right to left and is given by the upper horizontal scale), such that the displacement curves of the opening and closing (*lower lines*) coincide.

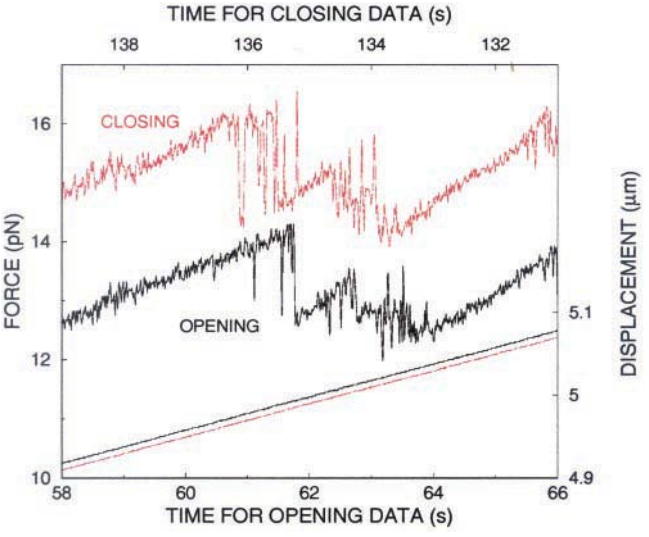

FIGURE 18 Detail of the force and displacement signals as a function of time. For the opening data (*dark lines*) time increases from left to right and is given by the lower horizontal scale. For the closing data (*red lines*) time increases from right to left and is given by the upper horizontal scale. For convenience, we have vertically upshifted (by 2 pN) the force signal recorded upon closing and have positioned opening and closing data horizontally, such that the displacement curves slightly separate and the features of the force curves closely coincide.

explained by our current theoretical description. To account for them theoretically, we would have to go beyond the assumption of thermal equilibrium.

In Fig. 18 a detail of the force curve is presented where the opening and closing signals show a rather close agreement. The corresponding theoretical results are shown in Fig. 19. We notice that, at this scale, the experimental force curves exhibit important differences compared to the calculated curve. The decreasing part of the sawteeth is smoother in the calculated force curve (Fig. 19, *upper line*) than in the measurement. In addition, force flips appear in the measured signal that are not borne out by the calculation. In Fig. 18, pronounced flips appear in the opening data in the time interval 60–64 s and for closing in the interval 133–137 s. The corresponding displacement interval (4.95–5.03 μm) is given by the displacement curves (*straight lines*, *right scale*). Such bistabilities are observed only at elevated stiffness (with the trapping interferometer but not with the soft microneedle), at low displacement velocity and in the vicinity of the decreasing part of a sawtooth. Under these conditions, sudden flips between force values are frequently observed and occur also without sample displacement (data not shown).

The amplitude of the force fluctuations on the measured curves of Fig. 18 exhibits a sizable variation with displacement. Qualitative agreement is obtained between the displacement dependence of the calculated force variance (lower curve of Fig. 19) and the amplitude of the measured fluctuations. The weak shoulder at $t = 59$ s (displacement of 4.94 μm) corresponds to an enhanced force fluctuation in experiment and theory. Maximum fluctuation occurs around the drop of the big sawtooth (around 61.5 s or 4.97 μm), again both in experiment and theory. The increased force fluctuations measured around $t = 63$ s are also predicted theoretically. The amplitude of the noise on the measured signal should not, however, be equated with the calculated value of var F, because the

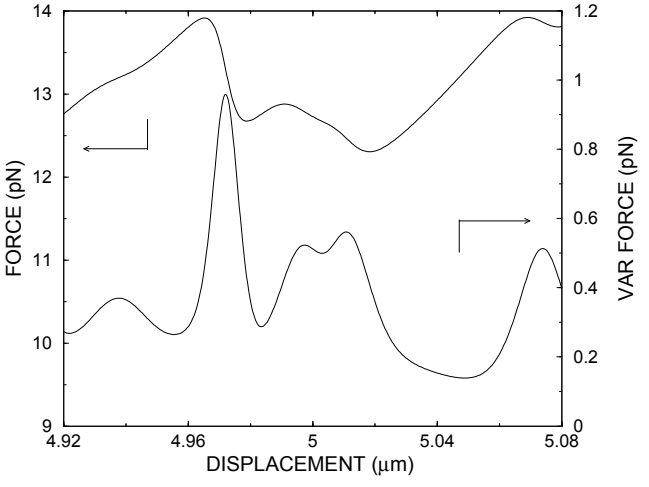

FIGURE 19 Calculation of the force F (*upper curve*) and the statistical variance in the force var F (*lower curve*) for the displacement interval of Fig. 18. The force variance is defined by var $F = \sqrt{\langle F^2\rangle - \langle F\rangle^2}$, where $\langle \ldots \rangle$ indicates the ensemble average (Eq. 12) of our theoretical description.

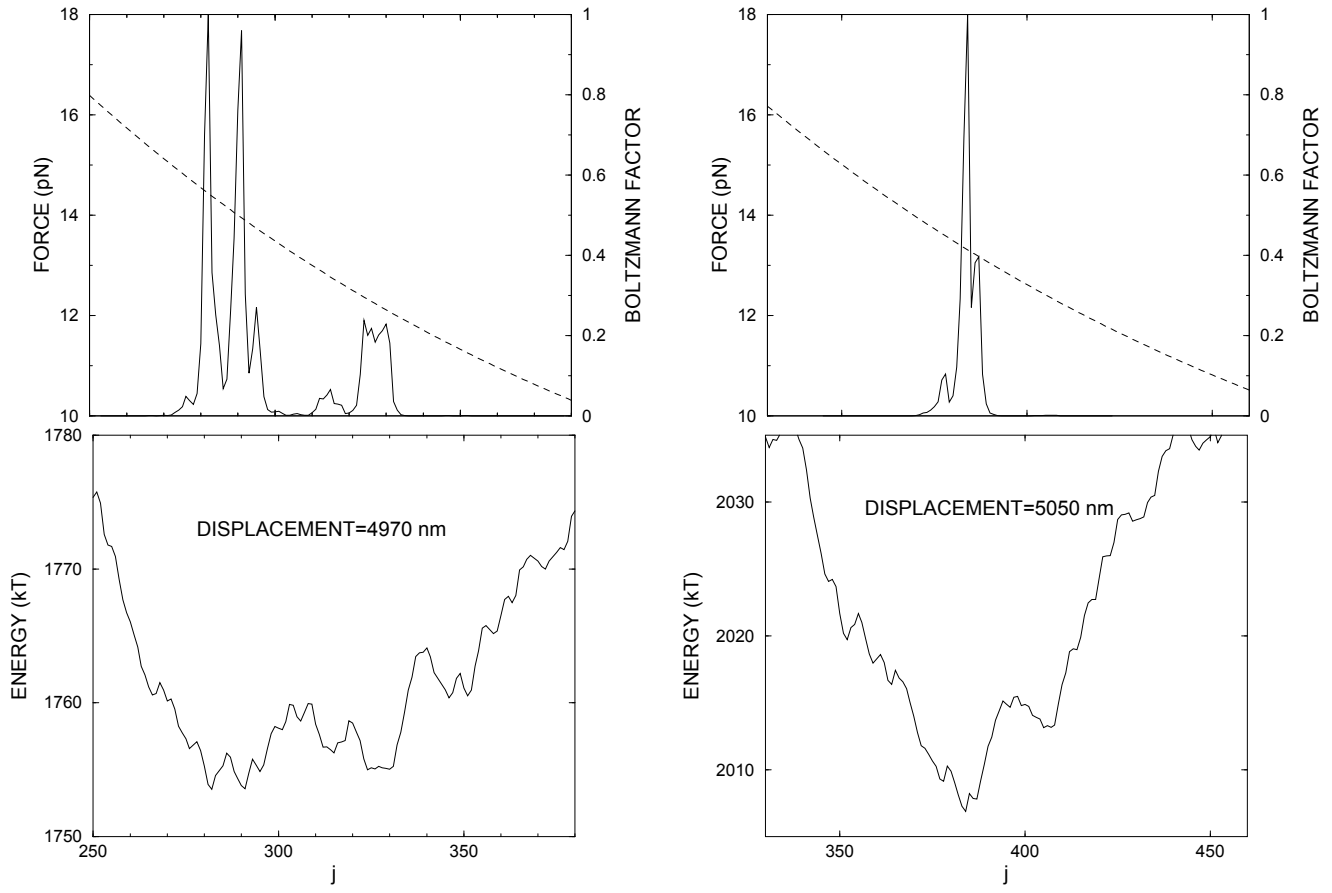

FIGURE 20 *Bottom*: Calculated energy landscape for a displacement of 4970 nm (*left*, corresponding to the rapidly decreasing part of a sawtooth in the force versus displacement curve) and for a displacement of 5050 nm (*right*, corresponding to the slowly rising part of a sawtooth). The presented energy includes the statistical averaging over the lengths δ_1 and δ_2 of the molecular construction (Eq. 12). *Top*: probability described by the Boltzmann factor $e^{-(E-E_{min})/k_BT}$ (*solid line*) and force (*dashed line*) as a function of j. Some average values corresponding to the figure. *Left*: $\langle j\rangle = 298$, var $j = 18.2$, $\langle F\rangle = 13.6$ pN, var $F = 0.88$ pN. Right part: $\langle j\rangle = 384$, var $j = 3.08$, $\langle F\rangle = 13.3$ pN, var $F = 0.14$ pN.

former is reduced by low-pass filtering and includes instrumental noise.

Fig. 20 illustrates our interpretation of the flips between different force levels. For a sample displacement corresponding to a position in the vicinity of the force drop of a sawtooth (left part, corresponding to ~61–62 s in Fig. 18, where there is a bistability in the signal), the total energy, presented as a function of the number j of opened basepairs, exhibits at least two local minima, which are close in energy and are separated by a potential barrier. One minimum corresponds to higher force and lower j, the other one to lower force and higher j, leading to a bistability of the opening fork. At slow displacement (or at fixed stage) and provided that the height of the potential barrier does not exceed a few k_BT, the system fluctuates thermally between the different minima, and therefore the Brownian motion resembles telegraph noise. Thermal equilibrium theory is appropriate if the system disposes enough time to exploit the whole relevant parameter space to establish the average value. If the imposed displacement velocity is too high, we expect differences between the force signals recorded upon opening and closing. Hysteresis may occur because during opening the system statistically remains longer close to the minimum of small j, while during closing it remains longer close to the minimum of higher j.

During the rising part of a sawtooth, corresponding to the "stick" phase of the molecular stick-slip motion, only a single minimum region is present in the energy landscape (right part of Fig. 20). In this case flips do not occur and, because there is no significant energy barrier, the thermal equilibrium average value is established more rapidly than during the "slip" phase. Therefore, we expect fewer differences between opening and closing signals in the "stick" phase than in the "slip" phase.

The numerical calculation that takes into account the DNA base sequence is necessary to correctly describe the energy landscape with the minima and potential barriers. In the central part of Fig. 18, flips occur with an amplitude of 1–2 pN and a typical repetition rate ν^{-1} of 10 Hz. The

transition time of a flip is not resolved, because it is below our experimental time resolution (~10 ms in this measurement). The measured force amplitude agrees favorably with the difference between the calculated forces corresponding to the two regions around $j \cong 290$ and $j \cong 330$ (Fig. 20, *top left*, *dashed line*). The calculation predicts a barrier of height $E_b = 4 - 5\ kT$ between these regions (Fig. 20, *bottom left*). Assuming a thermal activation across this barrier described by the expression $\nu = \nu_0 e^{-E_b/k_BT}$ with $\nu = 10$ Hz, we obtain a trial frequency ν_0 in the range 500–1500 Hz.

We now consider a simple theoretical description of the sudden flips in force, which is based on an analytical treatment of the molecular stick-slip motion described in section IV of Bockelmann et al. (1998). We neglect the complex energy landscape of the DNA sequence and assume that the energy needed to open a basepair of the double helix exhibits a descending step at basepair index $j = j_{step}$, but is constant elsewhere. This energy, given by $E_{a\nu} + \Delta/2$ for $j < j_{step}$ and $E_{a\nu} - \Delta/2$ for $j > j_{step}$, comprises the binding energy of the basepair and the elastic energy needed to stretch the opened basepair to the average opening force. In addition, we assume that the total stiffness (Eq. 14) is independent of j, a good approximation as long as the fluctuations of j around the average $\langle j \rangle$ are sufficiently small. Let us consider the case of a stage fixed at a position x_0 that corresponds to $\langle j \rangle = j_{step}$. Apart from a constant, the total energy can then be written as

$$E_{tot} = \frac{1}{2} k_{tot}(x_{step} - 2z_0 j_{rel})^2 + j_{rel}\left(E_{a\nu} \mp \frac{\Delta}{2}\right) \quad (15)$$

where k_{tot} and x_{step} are the total stiffness (Eq. 14) and the total length of all the elastic elements in series at the average opening force. The length z_0 is the length/base of a DNA single strand at the average opening force, $j_{rel} = j - j_{step}$, and the upper (lower) sign corresponds to positive (negative) j_{rel}. Thus, the rapidly varying energy landscapes, as shown, for instance, on the bottom part of Fig. 20, reduce to two quadratic parabolas that have the same curvature and are joined at $j = j_{step}$. The two minima of Eq. 15 have the same energy, are located at

$$j_{rel} = \pm \frac{\Delta}{8 k_{tot} z_0^2}, \quad (16)$$

and are separated by a potential barrier of height

$$h = \frac{\Delta^2}{32 k_{tot} z_0^2} \quad (17)$$

The corresponding difference in force is given by $\Delta/(2z_0)$. Our analytical description thus predicts a decrease in barrier height h with increasing stiffness, $h \sim k_{tot}^{-1}$, and an increase with increasing force difference, $h \sim \Delta^2$.

We now consider two numerical examples to get a feeling for the orders of magnitude involved in the measurements. In the optical trap experiment, the total stiffness, k_{tot}, defined by Eq. 14, is estimated to be ~0.02 pN/nm, as follows. A typical trap stiffness k_{trap} of the measurement is 0.25 pN/nm. The molecular stiffnesses at the opening force are derived from experiment. For the ds-DNA linker arms (~15,000 bp total) we have $k_{ds} \cong 0.03$ pN/nm. For an ss-DNA of 600 bases (corresponding to Fig. 19, $j = 300$) we have $k_{ss} \cong 0.17$ pN/nm. The length $z_0 = 0.5$ nm follows from the experimental progression of the opening fork with sample displacement (1 μm in displacement corresponds to opening 1000 basepairs on average). We take $\Delta = 1$ pN nm $= 0.25\ kT$, which gives a force difference $\Delta/(2z_0)$ of 1 pN. From Eq. 16 we then obtain a separation of the parabola in j by 50 basepairs, a value close to the result of the numerical calculation presented in Fig. 20 (*bottom left*). For the barrier height h, however, the analytical description predicts with 1.6 kT a value about three times smaller than the numerical result. This difference mainly confirms that the energy variation caused by the DNA base sequence is important and should be taken into account for a description of the local energy landscape. The analytical description combined with the scheme of simple thermal activation leads to a transition probability across the barrier that decreases exponentially with decreasing k_{tot}. This may explain why flips are not observed when unzipping DNA with soft microneedles. In those measurements we have $k_{tot} < 0.0015$ pN/nm ($k_{lever} = 0.0017$ pN/nm, $k_{ds} = 0.01$ pN/nm) and our model thus predicts a flip probability $>10^5$ times smaller than in the tweezer case. If the stiffness is low, two separate minimum regions, quasi-degenerate in energy, are still calculated, but their separation in j and the height of the barrier between them are increased with respect to the case of higher stiffness.

A quantitative description of the observed force flipping is certainly very complex. The flip frequencies are strongly dependent on the kinetic barriers for which thermodynamic free energy differences can only provide an estimate. Additional complications may arise from viscous friction of the molecule and the bead, force, and velocity dependencies of the unfolding pathways and energy landscapes, deviations from the simple thermal activated barrier crossing scheme, couplings between torsion and linear elasticity, transient secondary structures in the single strands, and others.

We also emphasize the difference between the occurrence of force flips and their experimental observation. For instance, our soft microneedles are particularly slow (typically 50–100 ms) in their response to a force change because they are bulky and involve important bending, a combination that can give rise to strong viscous friction. In the unzipping configuration, this can prevent the full exploration of the minimum regions of the energy landscape. These regions are particularly extended at low stiffness. Force flips occurring at frequencies above the detection bandwidth are not detected, but may occur. AFM cantilevers provide fast response and are comparatively stiff, with spring constants

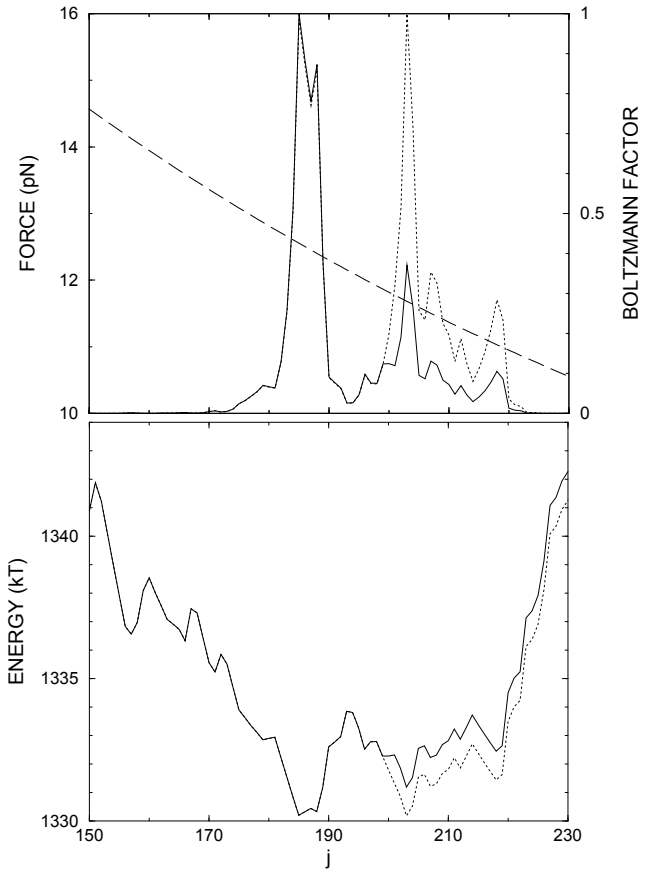

FIGURE 21 Same as Fig. 20, but for a displacement of 4838 nm, corresponding to the top of the small peak presented in the inset of Fig. 14. Energy landscape and Boltzmann factor are given for the case of the nonmutated sequence by dotted lines, for the case of the point mutation 189 C/G to A/T by solid lines. The mutation leads to a rigid upshift of the energy versus j curve starting at $j = 200$ (bp 189 of the λ-DNA appears at $j = 200$ in our molecular construction). The thermal averages are for the nonmutated case: $\langle j \rangle = 193$, var $j = 10.8$, $\langle F \rangle = 12.17$ pN, var $F = 0.51$ pN. With the mutation we have $\langle j \rangle = 198$, var $j = 11.7$, $\langle F \rangle = 11.93$ pN, var $F = 0.55$ pN.

of the order of 1000–10000 times higher than optical tweezers. Regarding our unzipping configuration, both optical tweezers and AFM cantilevers belong to a regime where the stiffness of the measurement device is high compared to the molecular stiffness. In this regime, the force flips are mainly determined by the molecular system itself and can be considered to a good approximation as independent of the force measurement device. Note, however, that mechanical perturbations of the setup may trigger flips; this type of external perturbation of the molecular system is expected to become more important with increasing stiffness.

A related force bistability has been observed recently by the group of C. Bustamante (Liphardt et al., 2001). Flips between folded and unfolded states that correspond to association/dissociation of ~20 basepairs are observed in optical tweezer measurements on single RNA molecules. The amplitude in force and the frequency of the flips in the RNA measurement are comparable to our DNA results. Such bistabilities have been observed with optical tweezers (the tweezer measurements on DNA and RNA correspond to a stiffness regime, which is intermediate between the one of AFM cantilevers and the one of soft microneedles), while we do not observe flips in unzipping DNA with soft glass microneedles.

Let us finally come back to the effect of mutations on the force signal. As shown in Fig. 14, an A → T mutation at base index $j = 189$ is predicted to almost erase the small peak at 4.8 μm in displacement. The corresponding effects on the energy landscape and the Boltzmann factor are presented in Fig. 21. We see that flips of ~1 pN in amplitude may occur at this position. With the mutation, the relative probability of the lower force level is reduced by a factor of three compared to the nonmutated case. This theoretical result suggests a scheme for the detection of the mutation, different from the measurement of the average force as a function of displacement. This alternative scheme consists in recording the force flips as a function of time at fixed stage (or very slow displacement) to measure the mutation-induced change in the probability distribution of the force values.

CONCLUSIONS

We have studied the opening and closing of DNA at slow displacement, corresponding to a close-to-equilibrium regime. Force measurements are performed with an optical trapping interferometer in a single molecule configuration and are compared to theoretical results. The force measurement setup with its calibration, and the sample preparation, with the molecular construction and the surface functionalization, are described in detail.

It is shown that the sensitivity of the force signal to the DNA sequence strongly increases with the total stiffness of the system. The combination of an optimized molecular construction and an optimized measurement technique results in a very significant improvement in basepair sensitivity with respect to our earlier work. Comparison of experiment and theory suggests that a part of the measured force signal corresponds to base sequence events appearing on a scale of <10 basepairs.

The quality of the agreement between different measurements and between experiment and the equilibrium theory varies along a force curve. Part of these differences are still due to instrumental limitations, but our results also indicate that thermal equilibrium is not always obtained in the measurements. This can induce statistical variations between the force signals. Local differences between opening and closing signals appear even at the lowest displacement velocity of 20 nm/s. At particular positions in the sequence we observe a characteristic flipping of the measured signal between discrete force levels. This behavior is explained by

transitions of the system between different minima in the complex energy landscape. The calculated statistical distribution of the corresponding force values depends strongly on the base sequence in the vicinity of the opening fork.

We thank D. Côte and P. Lopez for helpful comments on the manuscript.

This work was supported by the CNRS, the MENRT, and the universities Paris VI and Paris VII.

REFERENCES

Allemand, J. F., D. Bensimon, R. Lavery, and V. Croquette. 1998. Stretched and overwound DNA forms a Pauling-like structure with exposed bases. *Proc. Natl. Acad. Sci. U.S.A.* 95:14152–14157.

Allen, R. D., G. B. David, and G. Nomarski. 1969. The Zeiss-Nomarski differential interference equipment for transmitted-light microscopy. *Z. Wiss. Mikroskopie.* 69:193–221.

Allersma, M. W., F. Gittes, M. J. deCastro, R. J. Stewart, and C. F. Schmidt. 1998. Two-dimensional tracking of ncd motility by back focal plane interferometry. *Biophys. J.* 74:1074–1085.

Azzam, R. M. A., and N. M. Bashara. 1989. Ellipsometry and Polarized Light. North Holland, Amsterdam.

Bockelmann, U., B. Essevaz-Roulet, and F. Heslot. 1997. Molecular stick-slip motion revealed by opening DNA with piconewton forces. *Phys. Rev. Lett.* 79:4489–4492.

Bockelmann, U., B. Essevaz-Roulet, and F. Heslot. 1998. DNA strand separation studied by single molecule force measurement. *Phys. Rev. E.* 58:2386–2394.

Bustamante, C., S. B. Smith, J. Liphardt, and D. Smith. 2000. Single-molecule studies of DNA mechanics. *Curr. Opin. Struct. Biol.* 10: 279–285.

Clausen-Schaumann, H., M. Rief, C. Tolksdorf, and H. E. Gaub. 2000. Mechanical stability of single DNA molecules. *Biophys. J.* 78: 1997–2007.

Cluzel, Ph., A. Lebrun, C. Heller, R. Lavery, J.-L. Viovy, D. Chatenay, and F. Caron. 1996. DNA: an extensible molecule. *Science.* 271:792–794.

Cocco, S., R. Monasson, and J. F. Marko. 2001. Force and kinetic barriers to unzipping of the DNA double helix. *Proc. Natl. Acad. Sci. U.S.A.* 98:8608–8613.

Lee, G. U., L. A. Chrisey, and R. J. Colton. 1994. Direct measurement of the forces between complementary strands of DNA. *Science.* 266: 771–773.

Davenport, R. J., G. J. L. Wuite, R. Landick, and C. Bustamante. 2000. Single-molecule study of transcriptional pausing and arrest by *E. coli* RNA polymerase. *Science.* 287:2497–2500.

Denk, W., and W. W. Webb. 1990. Optical measurements of picometer displacements of transparent microscopic objects. *Appl. Opt.* 29: 2382–2391.

Essevaz-Roulet, B., U. Bockelmann, and F. Heslot. 1997. Mechanical separation of the complementary strands of DNA. *Proc. Natl. Acad. Sci. U.S.A.* 94:11935–11940.

Gittes, F., and C. F. Schmidt. 1998a. Interference model for back-focal-plane displacement detection in optical tweezers. *Optics Lett.* 23:1–3.

Gittes, F., and C. F. Schmidt. 1998b. Signals and noise in micromechanical measurements. *Methods Cell Biol.* 55:129–156.

Léger, J. F., J. Robert, L. Bourdieu, D. Chatenay, and J. F. Marko. 1998. RecA binding to a single double-stranded DNA molecule: a possible role of DNA conformational fluctuations. *Proc. Natl. Acad. Sci. U.S.A.* 95:12295–12299.

Léger, J. F., G. Romano, A. Sarkar, J. Robert, L. Bourdieu, D. Chatenay, and J. F. Marko. 1999. Structural transitions of a twisted and stretched DNA molecule. *Phys. Rev. Lett.* 83:1066–1069.

Liphardt, J., B. Onoa, S. B. Smith, I. Tinoco, Jr., and C. Bustamante. 2001. Reversible unfolding of single RNA molecules by mechanical force. *Science.* 292:733–737.

Lubensky, D. K., and D. R. Nelson. 2000. Pulling pinned polymers and unzipping DNA. *Phys. Rev. Lett.* 85:1572–1575.

Nelson, P. 1999. Transport of torsional stress in DNA. *Proc. Natl. Acad. Sci. U.S.A.* 96:14342–14347.

Odijk, T. 1995. Stiff chains and filaments under tension. *Macromolecules.* 28:7016–7018.

Rief, M., H. Clausen-Schaumann, and H. E. Gaub. 1999. Sequence-dependent mechanics of single DNA molecules. *Nat. Struct. Biol.* 6:346–349.

Sambrook, J., E. F. Fritsch, and T. Maniatis. 1989. Molecular Cloning: A Laboratory Manual. Cold Spring Harbor Laboratory Press, Cold Spring Harbor, New York.

SantaLucia, J. 1998. A unified view of polymer, dumbbell, and oligonucleotide DNA nearest-neighbor thermodynamics. *Proc. Natl. Acad. Sci. U.S.A.* 95:1460–1465.

Simmons, R. M., J. T. Finer, S. Chu, and J. A. Spudich. 1996. Quantitative measurements of force and displacement using an optical trap. *Biophys. J.* 70:1813–1822.

Smith, S. B., Y. Cui, and C. Bustamante. 1996. Overstretching B-DNA: the elastic response of individual double-stranded and single-stranded DNA molecules. *Science.* 271:795–799.

Smith, S. B., L. Finzi, and C. Bustamante. 1992. Direct mechanical measurements of the elasticity of single DNA molecules by using magnetic beads. *Science.* 258:1122–1126.

Strick, T. R., V. Croquette, and D. Bensimon. 2000. Single-molecule analysis of DNA uncoiling by a type II topoisomerase. *Nature.* 404: 901–904.

Svoboda, K., and S. M. Block. 1994. Biological applications of optical forces. *Annu. Rev. Biophys. Biomol. Struct.* 23:247–285.

Thompson, R. E., and E. D. Siggia. 1995. Physical limits on the mechanical measurement of the secondary structure of biomolecules. *Europhys. Lett.* 31:335–340.

Viovy, J.-L., Ch. Heller, F. Caron, Ph. Cluzel, and D. Chatenay. 1994. Sequencing of DNA by mechanical opening of the double helix: a theoretical evaluation. *C. R. Acad. Sci. Paris.* 317:795–800.

Wang, M. D., H. Yin, R. Landick, J. Gelles, and S. M. Block. 1997. Stretching DNA with optical tweezers. *Biophys. J.* 72:1335–1346.

Wuite, G. J. L., S. B. Smith, M. Young, D. Keller, and C. Bustamante. 2000. Single molecule studies of the effect of template tension on T7 DNA polymerase activity. *Nature.* 404:103–106.

Yin, H., M. D. Wang, K. Svoboda, R. Landick, S. M. Block, and J. Gelles. 1995. Transcription against an applied force. *Science.* 270:1653–1657.